Deliverable 15.10 Impact of bentonite-associated oxygen on microbial activity and viability

Work Package 15 ConCorD

This project has received funding from the European Union's Horizon 2020 research and innovation programme 2014-2018 under grant agreement N°847593.

Document information

Project Acronym	**EURAD**
Project Title	**European Joint Programme on Radioactive Waste Management**
Project Type	**European Joint Programme (EJP)**
EC grant agreement No.	**847593**
Project starting / end date	**1st June 2019 – 30 May 2024**
Work Package No.	**15**
Work Package Title	**CONtainer CORrosion under Disposal conditions**
Work Package Acronym	**ConCorD**
Deliverable No.	**15.10**
Deliverable Title	**Impact of bentonite-associated oxygen on microbial activity and viability**
Lead Beneficiary	**EPFL**
Contractual Delivery Date	**30/04/2024**
Actual Delivery Date	**07/05/2024**
Type	**Document**
Dissemination level	**Public**
Authors	**Natalia Jakus, Pranav Vivek, Stefano Mischler, Rizlan Bernier-Latmani**

To be cited as:

Jakus, N., Vivek, P., Mischler, S., Bernier-Latmani, R. (2024): Deliverable D15.10: Impact of bentonite-associated oxygen on microbial activity and viability. Final version as of 07/05/2024 of deliverable D15.10 of the HORIZON 2020 project EURAD. EC Grant agreement no: 847593.

Disclaimer

Acknowledgement

This document is a deliverable of the European Joint Programme on Radioactive Waste Management (EURAD). EURAD has received funding from the European Union's Horizon 2020 research and innovation programme under grant agreement No 847593.

Status of deliverable		
	By	Date
Delivered (Lead Beneficiary)	R. Bernier-Latmani	06/05/2024
Verified (WP Leader)	N. Diomidis	07/05/2024
Reviewed (Reviewers)	Birgitta Kalinowski, Fraser King, Mehran Behazin	22/04/2024
Approved (PMO)	……	……
Submitted to EC (Coordinator)	Andra (Coordinator)	07/05/2024

Executive Summary

In this report, we present the results of a 1.5-year-long borehole incubation experiment aimed at evaluating the persistence of oxygen in bentonite under anoxic conditions. Our focus was on the impact of oxygen on microbial viability and activity, as well as the mineralogical composition of the clay. To conduct the experiment, we used stainless steel modules filled with Wyoming bentonite compacted to 1.25 g/cm^3. Prior to deployment, the bentonite was equilibrated at varying initial oxygen saturation levels of 0%, 21%, and 100%. We also included a sterile control, where gamma-irradiated bentonite was exposed to 21% O_2. All modules contained carbon steel and copper coupons embedded within the clay. Our findings indicate that microbial growth occurred at all conditions, as demonstrated by 16S rRNA gene quantification. However, higher cell numbers were observed within the first 13 mm from the bentonite surface in direct contact with anoxic porewater. With decreasing oxygen levels, fewer bacterial cells were present, while concentrations of S, Fe(II), and Fe(total) increased within the clay. Magnetite and siderite were identified as the main reduction products using a combination of XRD, µXRF mapping, and the 6M-HCl extractions. We also observed carbon steel corrosion at all conditions, with the thickest layer of corrosion products observed for steel in contact with bentonite pre-treated with 21% O_2. Overall, our results demonstrate that both porewater- and bentonite-derived microbial communities contribute to the alteration of bentonite composition. This leads to the precipitation of sulphide phases and affects the stability of Fe(III)-bearing minerals, including the potential reduction of clays under conditions when O_2 is absent or completely consumed. Corrosion is most prominent in bentonite equilibrated at atmospheric O_2 due to a combination of simultaneous abiotic and biotic processes. Based on the qPCR data and the corrosion analysis combined, we propose that oxygen plays a crucial role in shaping microbial communities, and its decrease causes a shift towards less abundant but more specialized corrosion-inducing microorganisms. Our findings have important implications for the establishment of a microbial community within bentonite, happening most likely before full swelling of the clay when there is still an opportunity for bacterial growth.

Table of Contents

1. Introduction

It is known that sulphate-reducing bacteria (SRB) are present in bentonite, but long -term *in situ* incubation experiments showed that their number does not contribute significantly to the total number of anaerobic microorganisms in the clay, despite preferential growth conditions (no oxygen, the availability of sulphate and electron donors)(Burzan et al., 2022). A similar observation has been made in studies on Spanish clay (Martinez-Moreno et al., 2023; Povedano-Priego et al., 2023). This points towards the long-term persistence of O_2 (perhaps as an adsorbed gas) in bentonite, where oxygen would be expected to be consumed by abiotic processes (e.g., iron oxidation) or aerobic respiration shortly after subjecting the clay to reducing conditions. Therefore, in this Subtask, the hypothesis that O_2 bound in bentonite may inhibit SRB (which are strictly anaerobic microorganisms) is evaluated. The impact of O_2 would be relevant over relatively short-term periods during which the clay buffer starts to be saturated but has not fully swelled and there may be potential for microbial growth. While O_2 may be depleted during the longer periods relevant to the repository, allowing SRB to grow if conditions permit, the short-term effect was tested in a new in situ experiment at Mont Terri.

2. Methods

Experimental setup

Twelve stainless steel cylinder modules (mini-modules; 5.3 cm tall, 3.8 cm outer diameter) lined with a sintered, porous stainless steel filter and filled with Wyoming bentonite were placed in a larger module (25 cm tall, 12.6 cm outer diameter) identical to the one used in the IC-A experiment (e.g., Smart et al. 2017; Burzan et al. 2022), and incubated in-situ for 1.5 years in a borehole within Opalinus Clay at the Mont Terri Rock Laboratory. Each mini-module contained Wyoming MX-80 bentonite ground to < 30 mm and compacted to 1.25 g/cm^3 dry density, which prior to the assembly of the mini-modules was equilibrated (a) in the absence of O_2 for a year (0% O_2), or (b) in atmospheric O_2 (21% O_2), or (c) exposed to 100% O_2 for a year. Gamma-irradiated Wyoming MX-80 bentonite equilibrated to atmospheric O_2 (referred as 21% O_2-S) was included as a sterile control. Additionally, each module contained two metal coupons (small discs; 1.2 cm diameter, 0.3 cm thickness) made of carbon steel and copper embedded in the clay to monitor corrosion of the metals in response to the presence of O_2.

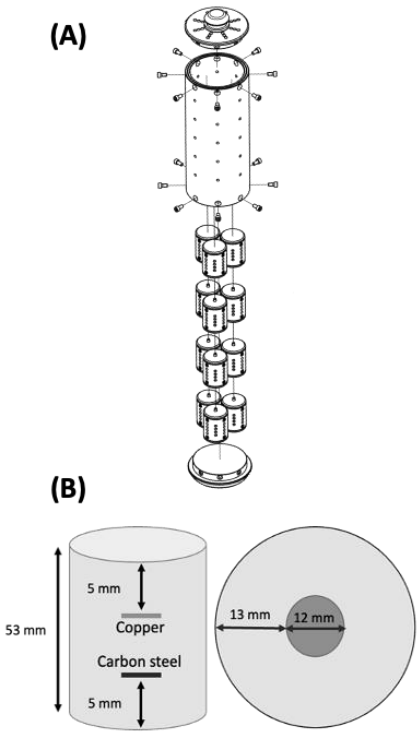

Figure 1: *(A) Module with twelve mini modules inside. (B) Placement of the metal coupons within the mini*

Modules retrieval and bentonite sectioning

After incubation, the module containing twelve mini-modules was retrieved from the borehole and immediately transferred to the anoxic glovebox (100% N_2) available at the site (Niche MA, Mont Terri Rock Laboratory). In the anoxic glovebox, the mini-modules were removed from the module and packed into Mylar® bags under anoxic conditions (100% N_2). Samples were then removed from the glovebox, transported to the laboratory and stored at 4°C until processing. The bentonite cores were recovered from the mini-modules using a sterile lever press and sectioned under sterile and anoxic conditions (100% N_2 glovebox). Each core was cut into three slices (1.5-2.0 cm thickness each) containing either: a copper coupon, carbon steel coupon, or the middle part of the core without a coupon. Maintaining anoxic conditions, the sections containing coupons were freeze-dried and embedded in a resin for corrosion characterization, while the middle sections of the cores were further sectioned using a sterile cylindrical tool to collect samples

representing the inner part of the core (2.51 cm diameter) and the outer layer (a ring of 1.29 cm thickness), and preserved at -20° C for gDNA enumeration, and air-, or freeze-dried under anoxic conditions for mineralogical characterization.

DNA extraction

DNA was extracted following methods described by (Engel et al., 2019b, 2019a) utilizing a modified protocol of DNeasy PowerMax Soil Kit (QIAGEN NV, Venlo, The Netherlands). Bentonite DNA was additionally purified by using 10 uL Invitrogen™Linear Acrylamide (5 mg/mL), 0.1 volume of 5 M NaCl and 2 volumes of isopropanol. The air-dried DNA pellets were resuspended in 40 µL elution buffer provided in the DNeasy® PowerMax® Soil Kit and stored at -20°C. Extracted DNA was quantified using an Invitrogen Qubit 2.0 fluorometer with 2 µL of extracted DNA and 198 µL of a working solution prepared by mixing Qubit™ buffer solution and fluorescent Qubit™ reagent following the standard protocol provided by the manufacturer.

16S rRNA gene copy quantification (qPCR)

Quantitative PCR (qPCR) analysis of the bacterial and archaean 16S rRNA gene was performed using the MYRA robotic system and a MIC qPCR Cycler (both BioMolecular Systems, Australia). Analyses were carried out in triplicate in 10 µL reactions. For quantification of the gene abundance, the following volumes of substrates were used: 2.5 µL template DNA, 2.1 µL water, 0.2 µL of each primer (100 mM stock) and 5 µL of 2× SensiFAST SYBR ® No-ROX Kit (Meridian Bioscience, UK). Samples were cycled (40 cycles) at 95 °C for 5 s, followed by an extension at 62 °C for 10 s and the acquisition at 72 °C for 5 s. The final melting step was carried out from 72 °C to 95 °C, at a rate of 0.1 °C/s. Analysis of the results was performed using the built-in analytical software (micPCR, BioMolecular Systems, ver. 2.12.6). Average efficiency (0.943 – 1.003) and r^2 values (> 0.99) were determined from seven points of the serial dilutions (10^7 –10^1 copies) for bacterial 16S rRNA gene. Based on calibration curves obtained using *E. coli* DNA, C_q values were used to calculate the gene copy numbers which were normalized against the mass (ng) of the extracted DNA. The primer pair used for the reaction to quantify bacterial 16S rRNA gene consisted of 338f: 5'-ACT CCT ACG GGA GGC AGC AG-3' and 534r: 5'-ATT ACC GCG GCT GCT GGC A-3'.

Fe extractions

The freeze-dried outer layers of the cores together with unreacted reference starting materials (Wyoming bentonite and gamma-irradiated Wyoming bentonite) were subjected to HCl extractions to quantify the iron phases. 0.5 M HCl is typically used to solubilize adsorbed and solid phase Fe(II) species, including siderite and green rust, and a reactive fraction of Fe(III) minerals (Fredrickson et al., 1998), while 6 M HCl is used to extract more crystalline iron phases such as poorly reactive sheet silicate Fe or FeS species (Heron et al. 1994; Poulton and Canfield 2005.) Before extractions, all glassware was kept in a 10% HCl bath overnight and rinsed 3x with distilled water and 3x with MilliQ water. In an anoxic glovebox (100% N_2), 0.5 g of dry clay was weighed into a 50-mL serum bottle with 10 mL extractant and N_2 headspace. Throughout the extraction, all samples were kept in the dark for 24h under anoxic conditions. Samples extracted with 0.5 M HCl were continuously shaken on a horizontal shaker at 100 rpm at room temperature, while samples mixed with 6 M HCl were kept anoxically in a 70 °C water bath. Following the extraction, 1 mL of sample was collected inside the glovebox at room temperature for 5 min at 13'500×g centrifugation and 20 uL of supernatant was collected for 50x dillution in anoxic 1 M HCl and Fe(II) and total Fe were quantified using the Ferrozine assay (Stookey, 1970). The concentration of Fe(III) was calculated by subtracting Fe(II) from total Fe.

X-ray diffractometry (XRD) and X-ray Fluorescence (XRF) analysis

XRD was performed using X'Pert MPD with X'Celerate equipped with a Cu-anode (Cu Kα radiation, λ = 0.15406 nm). Resulting diffractograms were analyzed using the software Match! (version 3.6.2.121) using reference patterns from the Crystallography Open Database (ver. COD-Inorg REV248644 2020.03.03). X-ray fluorescence spectroscopy maps of silicon (Si), sulphur (S) and iron (Fe; all K-edge) were obtained with an EDAX Orbis PCMicro EDXRF analyzer system (AMETEK Inc., Berwyn,

Pennsylvania, U.S.A.), equipped with a Rh micro-focus X-ray tube at 45kV acceleration and 1mA current and an Apollo XRF-ML50 Silicon Drift Detector. The spectra were recorded for 10 seconds at each spot with a step size of 30 um.

Bentonite water content

Bentonite water content and dry density were based on the wet weight and the dry weight after drying for 24 hours at 105°C. The dry weight of bentonite was used to normalize microbial and chemical data.

Corrosion analysis

The interface of metal coupons and bentonite, and the thickness and specific features of dense corrosion product layer (DPL) were investigated using Laser Confocal Optical Microscope Keyence (VK-X200) in a depth composition mode equipped with Nikon objective (20x0.46, OFN25, WD-3.1 mm). To calculate the DPL thickness, a minimum of 3 images at 20x and at least of 30 measurements of DPL thicknesses were taken and analyzed with ImageJ software. Renishaw inViva Confocal Raman microscope with 532 nm laser, 50X long distance lens at optimum laser power in the range of 20 mW was used to analyze the composition of DPL.

Statistical analysis

Analysis of Variance (ANOVA) at a significance level (alpha) of 0.05, was used to discern significant differences between the treatments. In instances where the ANOVA indicated significant differences existing within data sets, pairwise comparisons were conducted using the t-Student test for each individual pair at a significance level (alpha) of 0.0083, adjusted for multiple comparisons using the Bonferroni correction method.

3. Results and discussion

Microbial analysis

Quantification of the bacterial 16S rRNA gene provides evidence that oxygen acts as an important factor influencing the extent of microbial growth. During the incubation, growth was observed both inside the core and in the outer layer, with a lower number of gene copy number observed in the inner part of the cores across all the treatments (Figure 2). The lowest abundance of gene copy number inside the cores was found in the initially sterile bentonite (7.80E+03), while the highest was noted in 100% O_2 treatment (1.02E+05). Despite the overall small increase in the gene copy number inside the bentonite in all treatments, significant differences ($p < 0.05$) were found in 0% O_2 and sterile clay when compared to their corresponding starting materials, i.e., gene copy numbers in degassed clay and sterile clay used for the assembly of the mini-modules. Most of the microbial growth occurred in the clay outer layer (up to 1.29 cm distance from the bentonite surface in direct contact with porewater). The significant ($p < 0.0083$) differences were observed between growth in 0% and sterile 21% O_2 bentonite, in 0% and 21% O_2 bentonite, and sterile 21% and 21% O_2 bentonite, with on average, the lowest growth in the 0% O_2 treatment (4.16E+05).

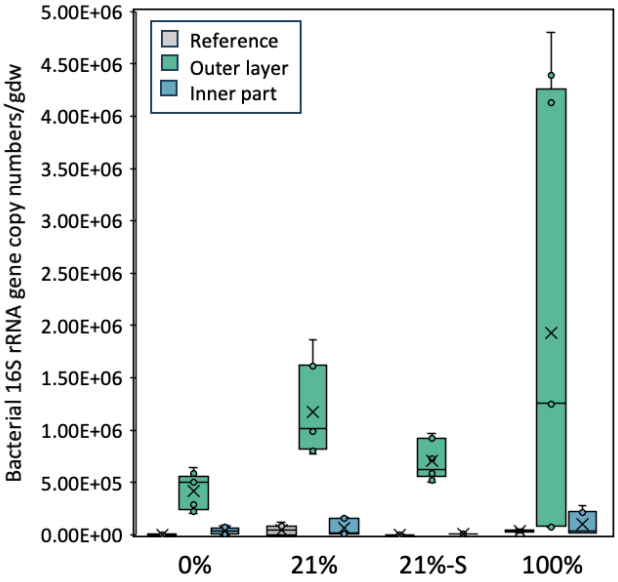

Figure 2: *16S rRNA gene V4 region amplicon quantification in bentonite after equilibration with varying O_2 concentrations and prior to deployment (grey) compared to number of gene copies in the bentonite after 1.5-year in-situ incubation. The data distinguish between bacterial growth in the outer (green) and inner (blue) parts of the bentonite cores. The horizontal line within the boxes represents the median, while 'X' shows the mean value. Whiskers are depicting minima and maxima outside the first and third quartiles. All results were standardized to dry weight of bentonite.*

Taken together, these observations lead to the conclusions that oxygen plays an important role in controlling the extent of microbial growth and likely shapes the identity of microbial communities through selection towards specific metabolic types. The lowest growth in oxygen-free bentonite suggests selection for anaerobic bacteria, while 21% oxygen allows for the growth of diverse or metabolically-flexible communities ranging from anaerobes to microaerophiles, with the highest growth observed in samples saturated with 100% oxygen, potentially promoting the growth of aerobes capable of consuming residual organic carbon present in clays. This observation, however, requires further support by using sequencing data that will allow for comparison of the microbial community profiles between the samples. Additionally, we observed that bacterial growth inside the compacted clay is limited and most likely corresponds to the growth of the 'indigenous' bentonite communities initially present in as-received clay. Interestingly, significant growth inside the sterile bentonite core may represent species that survived gamma irradiation. Moreover, most of the growth happens on the surface of the core, where more space for microbial growth could possibly be available, or inside the core, suggesting that bacteria originating from borehole water are capable of colonization of the bentonite.

Sulphate reduction

Micro X-ray Fluorescence (μXRF) analysis was used to trace the distribution of silicon (Si), iron (Fe) and sulphur (S). Si and Fe are indicative of the presence of clay minerals, such as montmorillonite (approximate formula $(Na,K,Ca)_{0.3}(Al, Mg, Fe, Ti)_2Si_4O_{10}(OH)_2 \cdot nH_2O$). Additionally, Fe is related to accessory minerals of Wyoming bentonite such as pyrite (FeS_2), siderite ($FeCO_3$) and iron-bearing clay minerals, or iron sulphide phases (Fe_xS_x) that could potentially form as a result of sulphate reduction. Sulphur (S) was used to trace sulphate present in Wyoming bentonite e.g. gypsum ($CaSO_4 \cdot 2H_2O$) or, similarly to Fe, sulphide being the products of sulphate reduction derived either from borehole water or the dissolution of sulphate-bearing minerals within bentonite. Si and Fe showed homogeneous distribution patterns mirroring their presence in clay minerals, while S distribution exhibited clear patterns reflecting the occurrence of black precipitates macroscopically visible on the outer layer of bentonite cores (Figure 3). More specifically, in the samples that were subjected to 0 and 21% O_2, S precipitates are present along the edge of the core and their concentration gradually decreases towards the middle. In case of samples equilibrated with 100% O_2, S is only present as single sulphur mineral phases within the clay matrix or on the surface of the bentonite core. Interestingly, the S distribution patterns among samples between 0-21% O_2 are unique for each treatment, with bentonite pre-conditioned with 0% O_2 being characterized by a broad band of S-containing phases with multiple single occurrences of high fluorescence intensity, sterile bentonite (21% O_2) showing a sharp boundary between the sulphur reduction front and possibly unaltered bentonite matrix, and 21% O_2 bentonite showing a broad band of S-containing phases of similar intensity fluorescence signal. These differences in S distribution patterns could be associated with the presence of sulphate-reducing bacteria, whose activity is limited by the presence of O_2. Interestingly, despite SRBs being strictly anaerobes, sulphate reduction can be observed in bentonites pre-conditioned at 21% of O_2, suggesting their tolerance to small levels of oxygen or depletion of O_2 that happened during incubation, allowing for the activity of anaerobic bacteria.

The sulphate reduction front is clearly present in the sterile control and differs from the sulphate precipitation pattern in the non-sterile sample equilibrated at the same O_2 concentration (21%). This suggests that the SRBs originating in the borehole water promote sulphide formation within bentonite with the integrated average rate of 1.55 mm/year either by their activity in the periphery (outside the bentonite) or within the bentonite (by colonizing it), or a combination of both. In the case of the activity of SRBs only in the periphery, the resulting HS^- diffuses into bentonite and precipitates in the form of Fe_xS_x. As available Fe(II) becomes progressively depleted, HS^- travels further inside the clay creating a band visible as S distribution in Figure 3B. In contrast, in the non-sterile controls, where bacteria are already present in bentonite, this front is shifted as the hotspots for sulphate reduction are dispersed within the clay reflecting the local presence of active bentonite-derived SRBs (Figure 3C). The S front in sterile samples could be also a result of the activity of SRBs originating from borehole water and that represent the extent of microbial bentonite colonization. The colonization of SRBs in this system is most likely limited by both the oxygen concentration and the ability of bacteria to migrate inside the bentonite.

Under *in-situ* conditions, the oxygen will be continuously consumed by abiotic processes and aerobic respiration, eventually leading to the establishment of conditions preferential for the activity of borehole water- and bentonite-derived SRBs. However, it is currently unknown if the growth of bacteria occurs only during the saturation and swelling phase, when more space is available, or also after the clay reaches the wet density that is inhibitory for microbial growth. In this case, the two opposing effect processes, i.e. oxygen removal (promoting) and swelling (inhibitory) would control microbial colonization and subsequent HS^- production. The nature of bacterial colonization and growth inside the bentonite was not a subject of this experiment and has to be addressed in separate study.

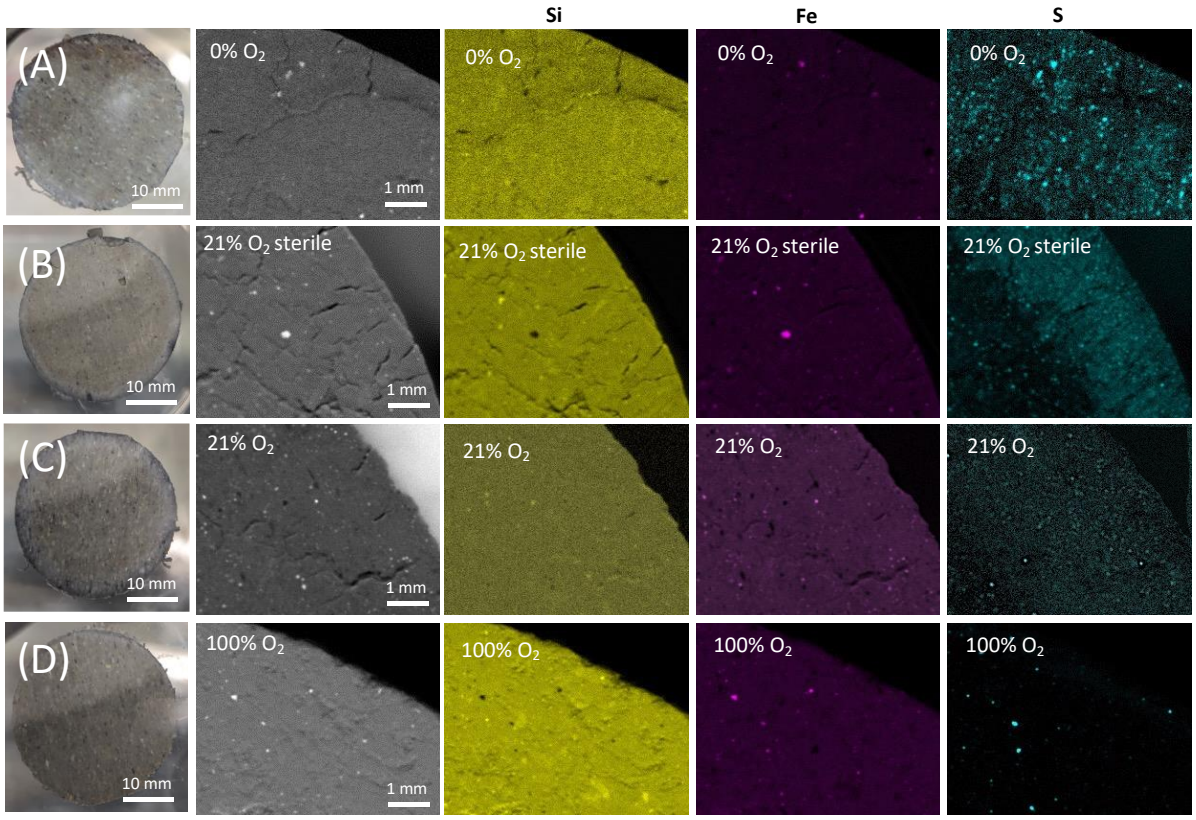

Figure 3: *Macroscopic pictures and XRF elemental distribution maps showing Si (yellow), Fe (purple) and S (blue) presence within the outer layer of the bentonite cores. Horizontal panels represent (A) 0% O_2, (B) 21% O_2 gamma-irradiated (sterile) (C) 21% O_2 and (D) 100% O_2 bentonite treatments. Accumulation of S represented as the distribution of bright blue spots in the last column differs for the four treatments, reflecting the sulphate reduction front within the bentonite and the contact with sulphate-containing borehole water.*

The Fe distribution maps do not mimic the behavior of sulphur, expected for the presence of iron sulphide phases. However, this is explained by the relatively high Fe background coming from Fe-bearing clays that potentially overwhelms the signal coming from iron sulphide.

Mineral composition analysis To follow the mineral changes in the outer layer of bentonite cores, X-ray diffraction was used. All samples showed mineral changes after 1.5 year incubation when compared to reference materials (as-received and gamma-irradiated bentonite; Figure 4). Mineral changes identified as the formation of magnetite (Fe_3O_4), goethite (α-FeO(OH)) and siderite ($FeCO_3$) occurred in bentonite equilibrated with 0% O_2. Additionally, diffraction patterns obtained from 21% O_2 sterile and 21% O_2 treatments show differences, suggesting that the presence and activity of microorganisms results in unique mineralogical changes in bentonite. Note that not all newly formed phases could be identified due to the complexity of the patterns and high background. The identity of sulphur-containing phases (most likely iron sulphide) found using μXRF mapping could not be identified most likely due to low relative abundance within the samples (detection limit between 1 - 5 wt%) or/and their poor crystallinity.

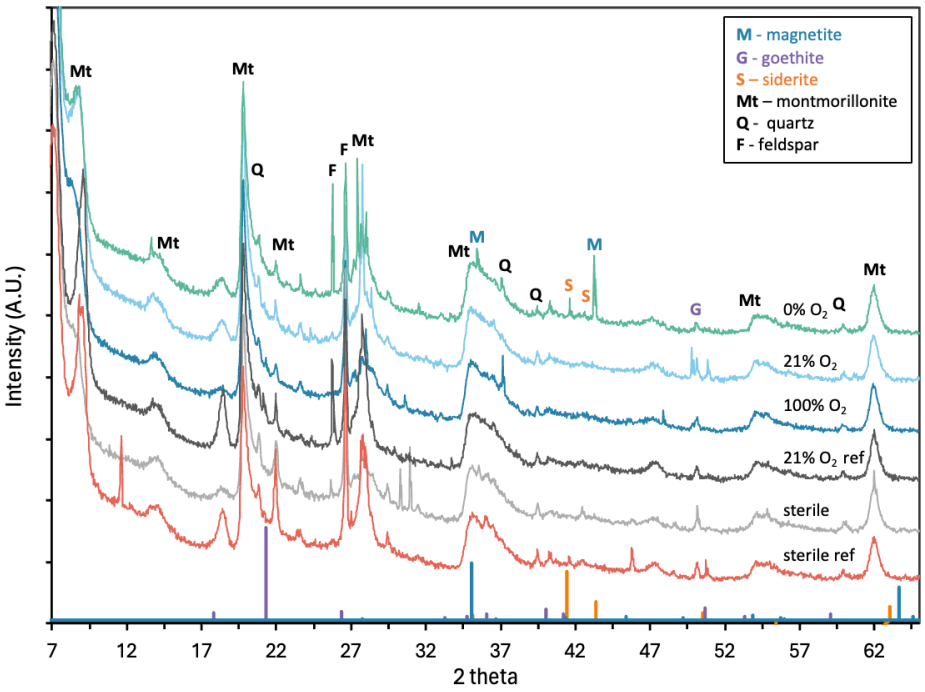

Figure 4: *Powder X-ray diffraction patterns of the reference (untreated) materials together with outer layers of the bentonite cores. Vertical lines (blue, purple and bright orange) at the bottom of the plot and corresponding to colored letters represent characteristic reflexes of new mineral phases in the samples identified as magnetite (M), goethite (G) and siderite (S). Black letters above the patterns show the main mineral constituents of untreated Wyoming MX-80 bentonite (montmorillonite, quartz, feldspar).*

To gather information about iron phases, HCl extractions were performed on the outer layers of the bentonite core samples. First, extractions in 0.5 M HCl representing readily extractable Fe(II) phases such as adsorbed Fe and siderite, showed that their composition has not changed regardless of the O_2 content yielding an average 1.95±0.32 mg/gdw of Fe(II) in all treatments including the

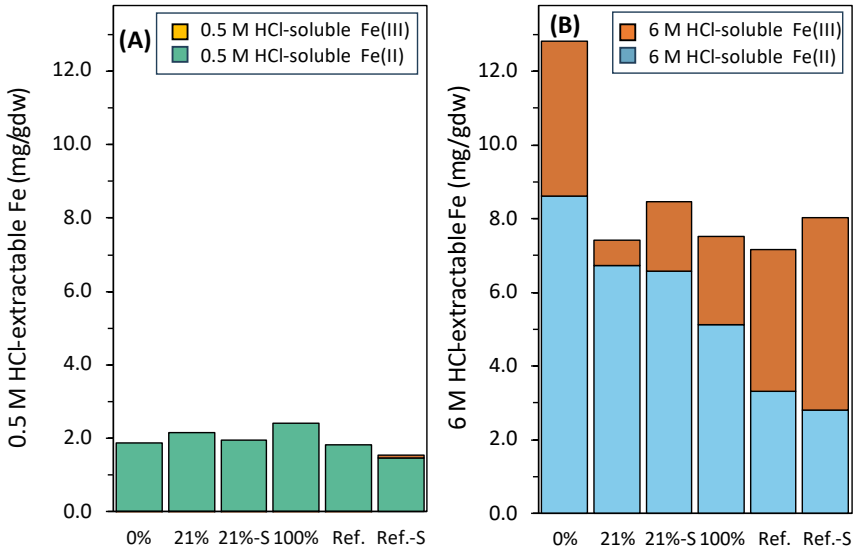

Figure 5: *Fe speciation in outer layer of bentonite cores determined by (A) 0.5 M HCl extraction representing readily extractable Fe(II), and (B) 6 M HCl extraction representing more crystalline iron phases such as poorly reactive sheet silicate Fe or FeS species reported in absolute values mg of Fe per gram of bentonite dry weight (mg/gdw).*

reference materials. Second, 6 M HCl extractions resulted in on average 7.00±0.47 mg/gdw of total Fe extracted from all the samples and reference materials except 0% O_2 sample that resulted in distinctively higher concentration of extractable total Fe (12.81 mg/gdw). This indicates that, in agreement with XRD data, the most changes in terms of mineral composition were induced in the complete absence of O_2 (0% O_2). Those mineral changes led to a decrease in the stability of Fe minerals, which might also include the stability of Fe-bearing sheet silicates for example by the reduction of clay minerals. Further investigation is needed to decipher the exact identity of impacted phases.

Fe(II) in as-received and sterile bentonite constitutes on average 40.6% of total 6M HCl extractable Fe. While under 100% O_2 it represents 68% and in 21% O_2, 90.5%, showing that the lower initial oxygen content in the clay, the higher the Fe(III) reduction rate. Additionally, the comparison of sterile vs. non-sterile treatment at 21% O_2 shows that bacteria already present in the clay enhance reduction converting nearly all available (6M HCl extractable) Fe(III) to Fe(II) phases.

Corrosion analysis

The extent of corrosion was assessed by analysis of two corrosion layers: the dense product layer (DPL), in direct contact with the metal coupon, usually consisting of crystalline corrosion product, and the transformed material (TM) characterized by the presence of poorly crystalline corrosion phases mixed with the bentonite matrix (Figure 6). All samples containing carbon steel coupons showed the presence of both corrosion layers, indicating that corrosion occurred at all conditions regardless of the initial O_2 content (Figure 7). Samples exhibited significant differences in the thickness of DPL with the

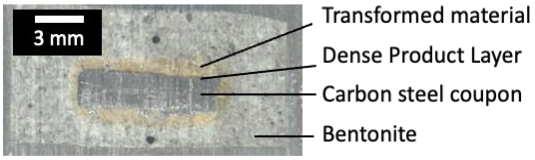

Figure 6: *A cross-section through a carbon steel coupon embedded in bentonite with corrosion products including dense product layer (DPL) and transformed material (TM).*

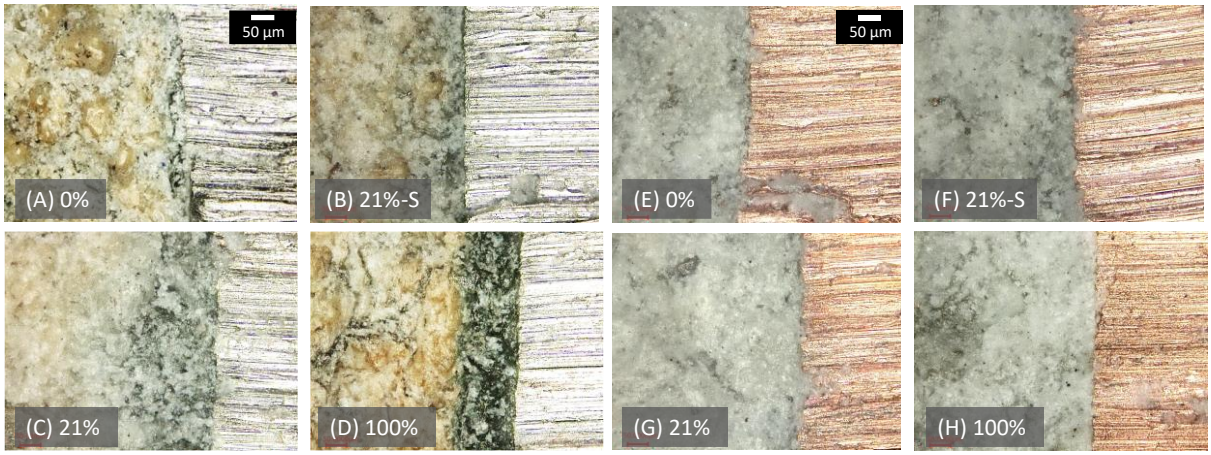

Figure 7: *Laser confocal microscopy images of clay-metal coupon interfaces at varying oxygen concentrations including (A, E) 0% O_2, (B, F) 21% O_2 gamma-irradiated (sterile) bentonite (C, G) 21% O_2 and (D, H) 100% O_2, after 1.5 year in-situ incubation. Images A-D represent samples containing carbon steel coupons with visible corrosion products, including Dense Product Layer (dark-grey mineral precipitates) and Transformed Material (orange color). Images E-H show samples containing copper coupons where no alteration of the bentonite-coupon interface was observed.*

lowest being observed in the sterile 21% O_2 bentonite and the highest in 21% bentonite, while the thickness of TM showed the opposite trend (Figure 8). This, together with microbial data on 16S rRNA gene quantification inside the bentonite core, indicates that microbes contribute to the formation of dense corrosion products. One of the possible differences in the thickness of TM could be explained by limitation in the diffusion of Fe from the coupon into the bentonite caused by the presence of microorganisms like Fe-metabolizing bacteria that potentially may impact the fate of Fe within the bentonite e.g., by the microaerophilic oxidation of Fe(II) or the reduction of Fe(III). The differences

between the thickness of DPL between 0%, 21% and 100% O_2 treatments with 21% having the highest thickness, could be explained by simultaneous contribution of abiotic O_2 oxidation of coupons and activity of sulphate-reducers (as supported by XRF observations), while under the 0% O_2 conditions, the oxidation of the coupon is related to the activity of microorganisms inducing corrosion, and under 100% O_2 condition, the corrosion is driven mostly abiotically, by oxygen. Interestingly, copper coupons did not show any indication of oxidation, even at 0% O_2 conditions where SRBs should be most active, which could be explained by either toxicity of Cu released from the coupons or that other groups of bacteria than SRB are crucial in oxidation process of phases present in the material selected for future canisters.

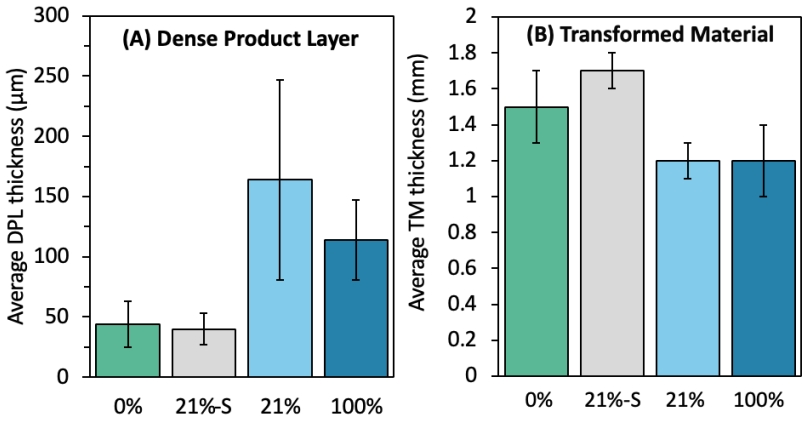

Figure 8: *Thickness of (A) Dense Product layer (DPL) and (B) Transformed Material (TM) measured at the interference of carbon steel coupons and bentonite with varying O2 concentrations: 0% O_2 (green), 21%-S O_2 gamma-irradiated bentonite (grey), 21% O_2 (pale blue) and 100% O_2 (dark blue) after 1.5 year in-situ incubation. Columns are representing average values while whiskers indicate standard deviation.*

Next, we intended to identify the corrosion products present in the DPL. µRaman spectra show the presence of both magnetite and goethite as the main products. While the XRD results only point to the formation of these two iron oxides for the 0% O_2 treatment, the µRaman analysis provides evidence for the formation of goethite and magnetite in all treatments.

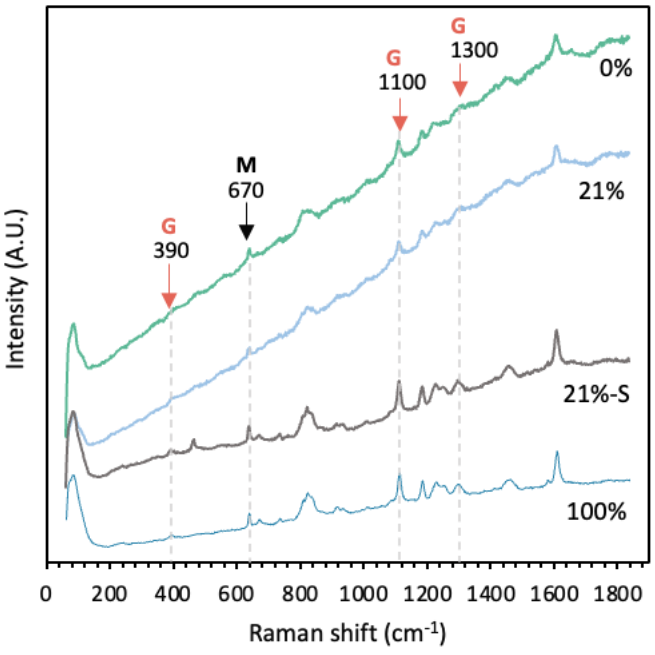

Figure 9: *µRaman spectra of DPL showing most corrosion product. Letters G and M indicate the characteristic peak positions for goethite and magnetite, respectively.*

4. Conclusions

Overall, the data obtained here evidence a key role for O_2 in stimulating the growth of (presumably aerobic) microorganisms in bentonite and inhibiting sulphate reducing ones. While these results await confirmation by microbial community fingerprinting, the emerging interpretation is that the presence of O_2 associated with bentonite inhibits the growth of indigenous sulphate reducing bacteria and possibly the colonization of SRB from the environment. This finding has implications for the establishment of a microbial community within bentonite. Indeed, it is expected that unless the dry density is high enough to preclude all microbial activity and growth, there is an opportunity for bacterial growth prior to full swelling of the clay and that if O_2 inhibits SRB growth, it may benefit the safety case by decreasing the potential for those organisms to build

biomass. This study was conducted using clay density lower than the commonly considered density that is inhibitory for bacterial activity (1.25 vs. 1.45 g/cm^3). However, the maintenance of homogenous density across the deposition tunnels in future repositories is challenging, which makes these results especially important for the areas of the backfill where the dry density is locally lower (the areas with heterogeneous distribution of density), for example, due to piping and erosion that may happen in the very early evolution of the repository (Leupin et al., 2014) or in excavation damaged zones. Additionally, this work evidences the microbially induced change in iron mineralogy in bentonite. At this stage, it is not clear whether this change in iron availability (as defined by HCl extractability) is linked to the formation of iron sulphide phases or whether it is simply due to microbial iron reduction. Community analysis will also help probe whether the growth of iron-reducing bacteria is detectable in various conditions.

5. References

Burzan, N., Lima, R.M., Frutschi, M., Janowczyk, A., Reddy, B., Rance, A., Diomidis, N., Bernier-Latmani, R., 2022. Growth and Persistence of an Aerobic Microbial Community in Wyoming Bentonite MX-80 Despite Anoxic in situ Conditions. Front. Microbiol. 13, 1–12. https://doi.org/10.3389/fmicb.2022.858324

Engel, K., Coyotzi, S., Vachon, M.A., McKelvie, J.R., Neufeld, J.D., 2019a. Validating DNA Extraction Protocols for Bentonite Clay. mSphere 4. https://doi.org/10.1128/msphere.00334-19

Engel, K., Ford, S.E., Coyotzi, S., Mckelvie, J., Diomidis, N., Slater, G., Neufeld, J.D., 2019b. Stability of Microbial Community Profiles Associated with Compacted Bentonite from the Grimsel Underground Research Laboratory. https://doi.org/10.1128/mSphere

Heron, Gorm., Crouzet, Catherine., Bourg, A.C.M., Christensen, T.H., 1994. Speciation of Fe(II) and Fe(III) in Contaminated Aquifer Sediments Using Chemical Extraction Techniques. Environ. Sci. Technol. 28, 1698–1705. https://doi.org/10.1021/es00058a023

Leupin, O.X., Karnland, O., Korkeakoski, P., Sellin, P., Mäder, U., Wersin, P., 2014. Montmorillonite stability under near-field conditions.

Poulton, S.W., Canfield, D.E., 2005. Development of a sequential extraction procedure for iron: implications for iron partitioning in continentally derived particulates. Chem. Geol. 214, 209–221. https://doi.org/10.1016/j.chemgeo.2004.09.003

Smart, N.R., Reddy, B., Rance, A.P., Nixon, D.J., Frutschi, M., Bernier-Latmani, R., Diomidis, N., 2017. The anaerobic corrosion of carbon steel in compacted bentonite exposed to natural Opalinus Clay porewater containing native microbial populations. Corros. Eng. Sci. Technol. 52, 101–112. https://doi.org/10.1080/1478422X.2017.1315233

Stookey, L.L., 1970. Ferrozine---a new spectrophotometric reagent for iron. Anal. Chem. 42, 779–781. https://doi.org/10.1021/ac60289a016